molecule has a roughly spherical body of which the diameter is approximately 2.8 Å.

Another interesting feature of this phase is that the tilting direction is opposite between the adjacent interlayer spaces. This implies that there is a correlation between the adjacent spaces. If the direction is the same, the sites designated by arrows in Figure 10 become close. Such an arrangement is unstable compared with the opposite case.

Registry No. K, 7440-09-7; hydrous titanium dioxide, 12214-43-6.

Contribution from the Institut für anorganische Chemie, CH-3000 Bern 9, Switzerland

Luminescence and Absorption Properties of VCl_2, $Mg_{1-x}V_xCl_2$, and $Cd_{1-x}V_xCl_2$ Crystals

BRIGITTE GÄLLI, ANDREAS HAUSER, and HANS U. GÜDEL*

Received September 24, 1984

Low-temperature luminescence and absorption spectra were recorded of VCl_2 doped into $MgCl_2$ and $CdCl_2$ as well as of the pure compound. There is evidence for excitation energy transfer in VCl_2 down to 5 K. In the diluted materials the luminescence remains unquenched up to 200 K ($Cd_{1-x}V_xCl_2$) and 250 K ($Mg_{1-x}V_xCl_2$). The broad-band $^4T_{2g} \rightarrow {}^4A_{2g}$ luminescence transition is highly structured in the diluted samples. There is multiple evidence for a Jahn–Teller effect in the $^4T_{2g}$ state with an estimated Jahn–Teller energy of the order of 200 cm^{-1}. Polarized absorption and Zeeman meausurements were used to assign the $^4A_{2g} \rightarrow {}^2E_g$, $^2T_{1g}$ transitions.

1. Introduction

The optical–spectroscopic properties of V^{2+} compounds have not received as much attention as those of other divalent transition-metal ions of the first series. V^{2+} has a $3d^3$ electron configuration like Cr^{3+}. But there is a significant difference between the two ions as far as their spectroscopic properties are concerned. In a large majority of Cr^{3+} complexes the first electronically excited states are ^2E_g and $^2T_{1g}$. Only in an environment that produces a small ligand field is there a sufficient lowering of $^4T_{2g}$, so that broad-band luminescence from that state can be observed. There is a great deal of current interest in systems with broad-band luminescences in the near-infrared (near-IR). One of the main aims is a search for compounds that may be brought to lase with a potential for tunability.[1-3] A number of crystalline and glassy materials that exhibit broad-band Cr^{3+} laser action have been developed and investigated in recent years.[1,4] In V^{2+} compounds the $^4T_{2g}$ state is the lowest, potentially luminescent, state in almost all environments. $^4T_{2g} \rightarrow {}^4A_{2g}$ luminescences have been observed for V^{2+} doped into $KMgF_3$, MgF_2, and $CsMgCl_3$ as well as for pure $CsVCl_3$.[5-7] Laser action was observed for the MgF_2 host lattice.[6] Encouraged by our observation that nonradiative relaxation processes could not compete with the luminescence process in $CsMg_{1-x}V_xCl_3$ up to room temperature,[7] we decided to study the spectroscopic properties of the title compounds.

The MCl_2 compounds used in this study all exhibit closely related layer structures, VCl_2 crystallizing in space group D_{3d}^3 and the host lattices $MgCl_2$ and $CdCl_2$ in space group D_{3d}^5. The M–Cl distance is 5% larger in $CdCl_2$ than in $MgCl_2$ and VCl_2.[8] The MCl_6 units are very close to octahedral, with $CdCl_2$ showing the largest trigonal compression. VCl_2 is an example of a two-dimensional Heisenberg antiferromagnet with a relatively large intralayer exchange coupling constant, $2J = -30$ cm^{-1}.[9] It undergoes a transition to three-dimensional magnetic order at 36 K,[10] but short-range magnetic order within the layers extends to much higher temperatures. Axial absorption spectra of VCl_2 and $Cd_{1-x}V_xCl_2$ have been reported in the literature.[11,12] In the present study we focus our attention on the $^4A_{2g} \leftrightarrow {}^4T_{2g}$ transitions, particularly in luminescence, and the fine structure in the region of ^2E_g, $^2T_{1g}$ excitations.

Table I. Crystal Field Parameters Derived from the Position of the Observed Absorption Bands[a]

compd	D_q, cm^{-1}	β	K, cm^{-1}	ζ, cm^{-1}
VCl_2	935	0.69		
$Cd_{1-x}V_xCl_2$	900	0.70	−210	100
$Mg_{1-x}V_xCl_2$	930	0.72	−270	100

[a] For crystal field calculations (weak field) the free ion energies were reduced by the factor β.

2. Experimental Section

2.1. Synthesis and Crystal Growth. VCl_2 was prepared by mixing stoichiometric quantities of VCl_3 (Cerac, 99.7%) and V powder (Merck, zur Synthese) in a quartz tube that was sealed under vacuum and slowly heated to 800 °C.[13] The few resulting platelet crystals were collected, and the grey-green powder was sublimed in a temperature gradient 1050 → 900 °C to yield another crop of green crystals. $CdCl_2$ (Pierce + Warriner suprapur) and $MgCl_2$ (Great Western Inorganics suprapur) were dried by heating them slowly under vacuum until they sublimed at 500 and 600 °C, respectively. The colder end of the tube was at 30 °C. The resulting powders were filled into quartz ampules with the desired amount of VCl_2 added. Single crystals were grown by the Bridgeman technique, the furnace being heated to 640 °C for the $CdCl_2$ and to 780 °C for the $MgCl_2$ host.

We always obtained crystals with a noticeable gradient in vanadium concentration due to the large difference in melting points of host and dopant. We did not succeed in growing crystals containing more than 5% of vanadium. Due to the two-dimensional structure of the crystals, plates with faces perpendicular to the crystal c axis could easily be cleaved. Samples with surfaces parallel to the optical axis were difficult to obtain. The products were very hygroscopic. They were checked by means of X-ray powder diffraction. The vanadium concentration of the doped samples was measured by atomic absorption spectrometry.

(1) Kenyon, P. T.; Andrews, L.; McCollum, B.; Lempicki, A. *IEEE J. Quantum Electron.* **1982**, *QE-18* (8), 1189.
(2) Johnson, L. F.; Dietz, R. E.; Guggenheim, H. J. *Appl. Phys. Lett.* **1964**, *5* (2), 21.
(3) Johnson, L. F.; Guggenheim, H. J.; Bahnck, D. *Opt. Lett.* **1983**, *8* (7), 371.
(4) Walling, J. C.; Peterson, O. G.; Jenssen, H. P.; Morris, R. C.; Wayne O'Dell, E. *IEEE J. Quantum Electron.* **1980**, *QE-16* (12), 1302.
(5) Sturge, M. D. *Solid State Commun.* **1971**, *9*, 899.
(6) Johnson, L. F.; Guggenheim, H. J. *J. Appl. Phys.* **1967**, *38*, 4837.
(7) Hauser, A.; Güdel, H. U. *J. Lumin.* **1982**, *27*, 249.
(8) Wyckoff, R. W. G. "Crystal Structure"; Interscience: New York, 1965.
(9) Cros. C.; Niel, M.; Le Flem, G.; Pouchard, M.; Hagenmuller, P. *Mater. Res. Bull.* **1975**, *10*, 461.
(10) Hirakawa, K.; Kadowaki, H.; Ubukoshi, K. *J. Phys. Soc. Jpn.* **1983**, *52* (5), 1814.
(11) Smith, W. E. *J. Chem. Soc. A* **1969**, 2677.
(12) Kim, S. S.; Reed, S. A.; Stout, J. W. *Inorg. Chem.* **1970**, *9* (6), 1584.
(13) Hauser, A.; Falk, U.; Fischer, P.; Güdel, H. U. *J. Solid State Chem.* **1985**, *56*, 343.
(14) Moore, C. E. "Atomic Energy Levels"; National Bureau of Standards: Washington, DC, 1952.

0020-1669/85/1324-2271$01.50/0

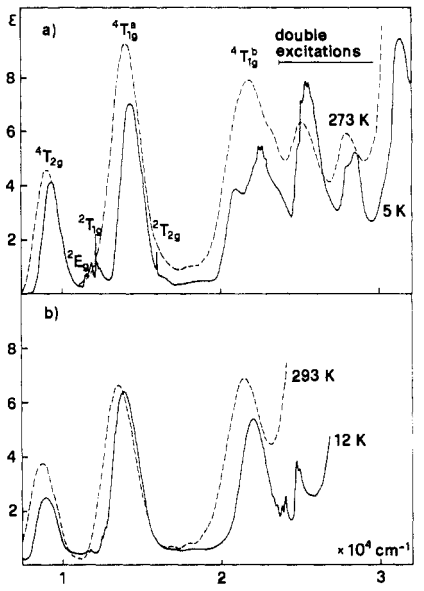

Figure 1. Axial absorption spectra of VCl_2 (a) and $Cd_{0.95}V_{0.05}Cl_2$ (b).

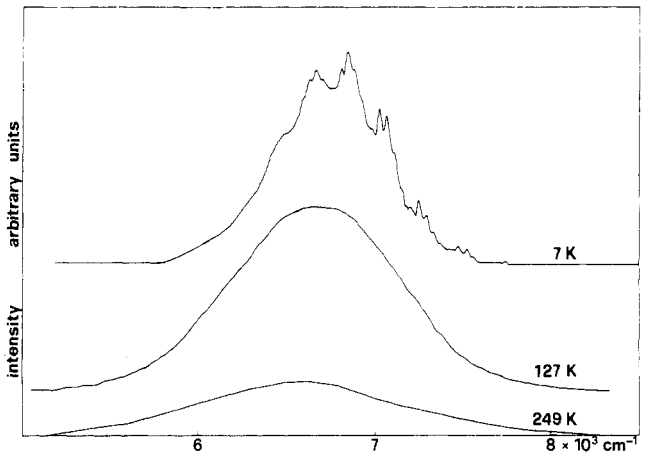

Figure 2. Temperature dependence of the unpolarized luminescence spectrum of $Cd_{0.998}V_{0.002}Cl_2$.

2.2. Spectroscopic Measurements. Low-resolution optical absorption measurements were performed on a Cary 17, equipped with a red-sensitive GaAs PM tube. For high-resolution transmission experiments we used a 100-W halogen lamp as a source, a $^3/_4$-m Czerny Turner monochromator (Spex 1702) with a grating blazed at 750 nm, and a cooled RCA 31034 photocathode detector.

For the luminescence experiments the crystals were excited with a xenon arc lamp (Varian VIX 150 UV) using suitable filters (broad-band excitation). The emitted light was dispersed by the Spex 1702 monochromator equipped with a grating blazed at 1.25 μm. The detection system consisted of a light chopper, a cooled PbS cell, and a lock-in amplifier. The samples were cooled by a helium gas flow technique. Magnetic fields of up to 5 T and temperatures down to 1.5 K could be reached by using a cryomagnet (Oxford Instruments, Spectromag 4).

3. Results

Figure 1 shows the absorption spectra of pure VCl_2 and $Cd_{0.95}V_{0.05}Cl_2$ at room and liquid-helium temperature. The spin-allowed bands are similar in the pure and dilute crystals, but the intensities of spin-forbidden transitions are seen to be much stronger in the concentrated compound. Double excitations involving the spin-forbidden ^2E_g, $^2T_{1g}$, and $^2T_{2g}$ transitions are as intense as the spin-allowed bands in VCl_2. Table I lists the crystal field parameters which reproduce the observed transition energies.

Infrared luminescence was measured of VCl_2 and weakly doped $MgCl_2$ and $CdCl_2$ samples. The maxima of the 7 K emission bands have energies of 7000, 7200, and 6500 cm^{-1}, respectively. Figure 2 reproduces, as an example of a dilute crystal, the luminescence sectrum of $Cd_{0.998}V_{0.002}Cl_2$. The broad-band emission is richly structured at 7 K and then broadens and loses intensity

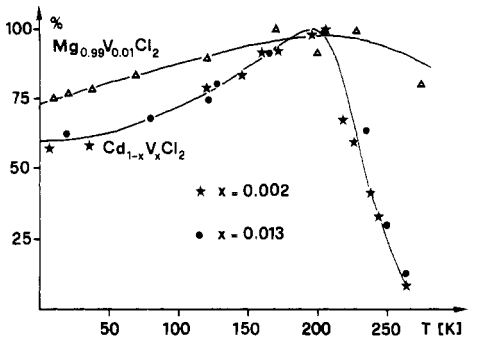

Figure 3. Temperature dependence of the V^{2+} luminescence intensity in the $MgCl_2$ and $CdCl_2$ host lattices.

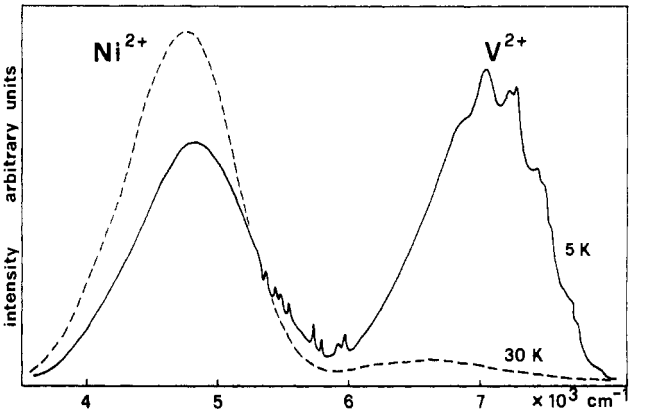

Figure 4. Unpolarized luminescence spectrum of nominally pure VCl_2 at 5 and 30 K. Both V^{2+} and Ni^{2+} emissions are indicated.

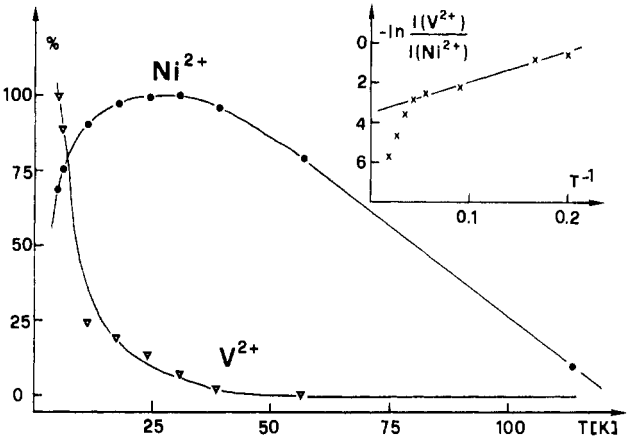

Figure 5. Temperature dependence of V^{2+} and Ni^{2+} luminescence intensities in VCl_2. The highest observed intensity is defined as 100% for each band separately. A logarithmic plot of the intensity ratio vs. inverse temperature is given as an insert.

with increasing temperature. This dependence of V^{2+} luminescence intensity on temperature is shown in Figure 3 for both host lattices. The behavior does not appear to depend on the vanadium concentration within the examined limits, but the nature of the host lattice plays an important role. In both lattices there is an increase of luminescence intensity between 10 and 200 K. The $Cd_{1-x}V_xCl_2$ emission then drops very steeply between 200 and 270 K, while the $Mg_{1-x}V_xCl_2$ luminescence remains practically unquenched up to 280 K.

The situation is entirely different for pure VCl_2. Broad-band luminescence is observed only at low temperature, decreasing rapidly when the temperature is raised. A second broad emission band, centered at about 4800 cm^{-1} and identified as a Ni^{2+} emission (section 4), quickly gains intensity with increasing temperature and then vanishes, also. Figure 4 shows the two luminescence transitions at 5 and 30 K. The temperature dependence of intensity for both bands is given in Figure 5. Both bands

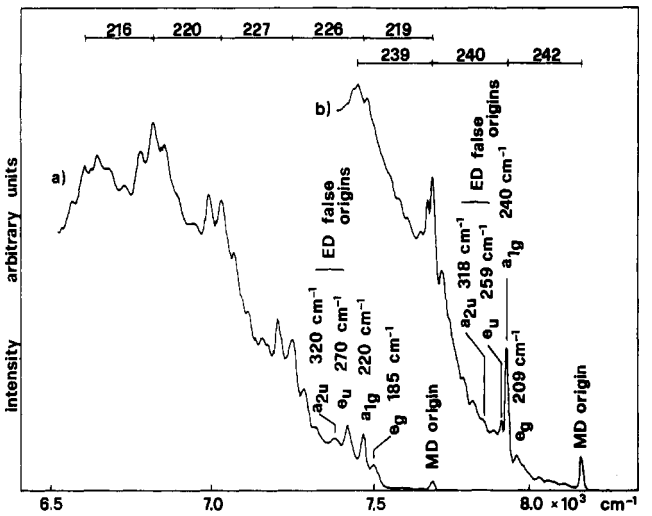

Figure 6. Fine structure of the V^{2+} luminescence at 6 K in $Cd_{0.998}V_{0.002}Cl_2$ (a) and $Mg_{0.99}V_{0.01}Cl_2$ (b). Electronic origins and vibrational sidebands are indicated (D_{3d} notation).

show some fine structure at 5 K. A progression in a mode of approximately 230 cm^{-1}, corresponding to a_{1g},[15] is the dominant feature in the V^{2+} band.

A great deal of fine structure can be seen in the 6 K spectra of the dilute systems, as depicted in Figure 6. The most prominent feature in the $Cd_{0.998}V_{0.002}Cl_2$ spectrum is the clear progression of a group of four bands with a period of approximately 220 cm^{-1}, corresponding to a_{1g}. The line at 7737 cm^{-1} is identified as a (magnetic dipole) electronic origin. The first group of four sidebands is indicated in Figure 6. They correspond to the first members of a progression in e_g and a_{1g} as well as two false origins of the e_u and a_{2u} (D_{3d} notation) enabling modes. Magnetic and electric dipole mechanisms make similar contributions to the total intensity of the band. In $Mg_{0.99}V_{0.01}Cl_2$ the origin is located as 8225 cm^{-1}, with an associated totally symmetric 240-cm^{-1} progression dominating the fine structure. The beginning of an e_g progression is also observed in this material. e_u and a_{2u} false origins are much weaker than in the $CdCl_2$ host, so that the total band intensity has more magnetic than electric dipole character. In $Mg_{0.99}V_{0.01}Cl_2$ the origin was shown under high resolution to consist of four component lines. Their total splitting is 19 cm^{-1}. They are reproduced for various temperatures between 7 and 20 K in Figure 7. The relative intensity of the higher energy components increases with increasing temperature, thus identifying the splitting as an excited-state splitting, as expected.

Figure 8 presents a detailed picture of the ^2E_g and $^2T_{1g}$ excitations in VCl_2 and $Cd_{1-x}V_xCl_2$ at low temperatures. The concentration dependence in the spectra of the dilute crystals suggests that all the prominent lines correspond to single-ion absorption processes. In the spectrum of a highly doped crystal we found new signals that are presumably due to pair excitations. But they were much too broad to provide information about exchange interactions. The ^2E_g, $^2T_{1g}$ transitions are more intense by 1–2 orders of magnitude in pure VCl_2. This is a clear indication that exchange mechanisms play a dominant part here. The bands are also much broader than those in the diluted samples. The two bands located at 11 470 and 12 150 cm^{-1} are sharper than the remainder of the spectrum. They show very peculiar variations with temperature. This is shown for the 11 470-cm^{-1} band in Figure 9. The intensity drops to zero between 30 and 40 K.

Figure 10 shows polarized absorption spectra of the bands A–D in Figure 8. They are compared with calculated intensity ratios[16] for the transitions $^4A_{2g} \rightarrow {}^2E_g$, split by the trigonal field and spin–orbit coupling into $\bar{E}$, $2\bar{A}$ (bands A and B), and the corresponding e_u false origins (bands C and D). The true origins are seen to have magnetic dipole character as expected, whereas the false origins are electric dipole transitions. Considering some depolarization in the σ and π spectra due to imperfect crystal

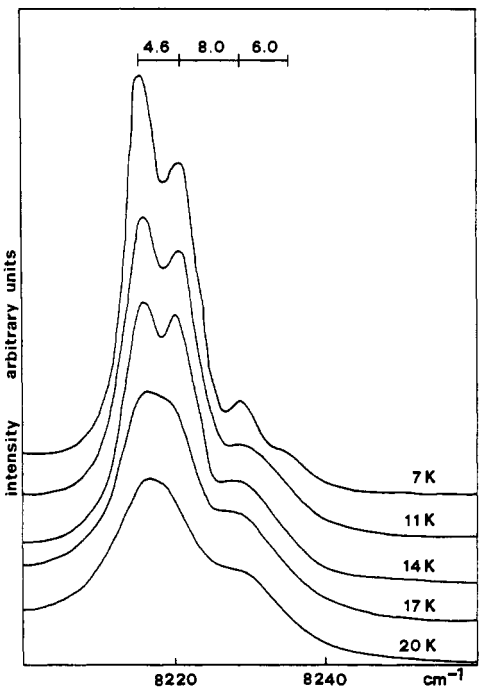

Figure 7. Spin–orbit split electronic origins of the $^4T_{2g} \rightarrow {}^4A_{2g}$ transition in the high-resolution luminescence spectrum of $Mg_{0.99}V_{0.01}Cl_2$.

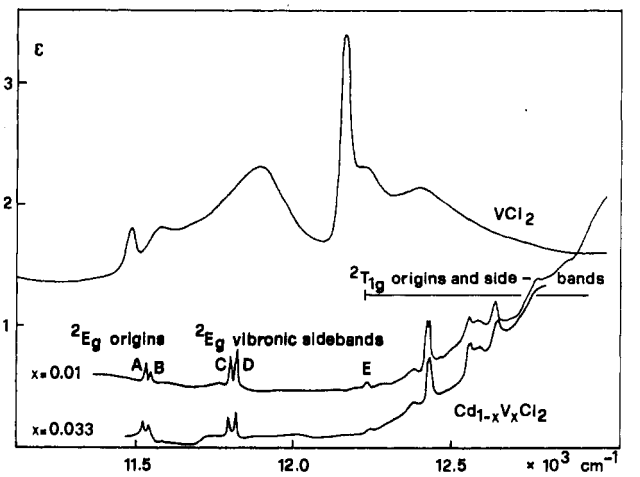

Figure 8. High-resolution absorption spectra of the $^4A_{2g} \rightarrow {}^2E_g$, $^2T_{1g}$ region in VCl_2 (5 K) and $Cd_{1-x}V_xCl_2$ (12 K).

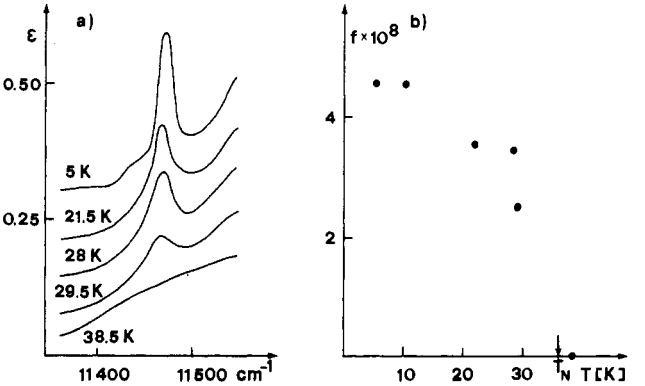

Figure 9. Temperature dependence of the 11 470-cm^{-1} $^4A_{2g} \rightarrow {}^2E_g$ magnon sideband in the axial absorption spectrum of VCl_2. f is the oscillator strength.

(15) Bauhofer, W.; Güntherodt, G.; Anastassakis, E.; Frey, A.; Benedek, G. *Phys. Status Solidi B* **1975**, *71*, 537.
(16) Sugano, S.; Tanabe, Y.; Kamurura, H. "Multiplets of Transition Metal Ions in Crystals"; Academic Press: New York, 1970.

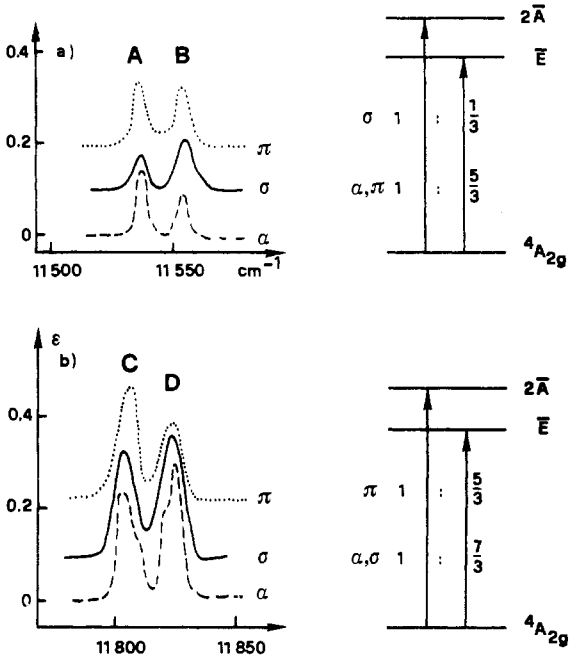

Figure 10. Polarized $^4A_{2g} \rightarrow {}^2E_g$ absorption spectra of $Cd_{0.99}V_{0.01}Cl_2$ at 12 K: (a) electronic origins; (b) e_u vibronic sidebands. Intensity ratios, calculated by a simple crystal-field model,[16] are given on the right-hand side.

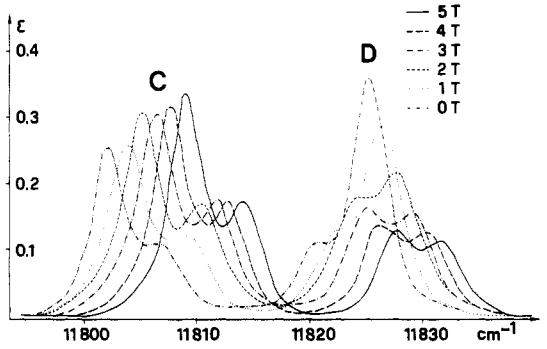

Figure 11. High-resolution Zeeman absorption spectra of the vibronic sidebands C and D (Figure 8) at 1.8 K (α spectrum, $H \perp c$).

surfaces, the agreement between experimental and theoretical intensity ratios is remarkable.

A further confirmation of these assignments was obtained from Zeeman absorption measurements on lines A–D. As an example Figure 11 shows the behavior of the false origins C and D, which are seen to have shoulders under high resolution, in a magnetic field perpendicular to the optical axis. There is a shift proportional to the field strength, accompanied by an intensity redistribution in the high-energy pair of lines. The electronic origins show the same energy shift. In combination with the known g values in the ground state[17] we can thus determine the excited-state g values. They are listed and compared with the values obtained from a crystal-field calculation in Table II. The agreement is good.

4. Discussion

4.1. Radiative and Nonradiative $^4A_{2g} \leftrightarrow {}^4T_{2g}$ Processes. Luminescence is much more informative than absorption in this spectral range. It exhibits a great deal of fine structure and shows pronounced changes with temperature. An interpretation of these effects provides a reasonable picture of the emitting states on the one hand, and some insight into the nonradiative processes competing with luminescence on the other hand.

We first discuss the observed temperature dependences. In the diluted crystals (Figure 3) there is an increase of luminescence

(17) Chan, L. Y.; Doetschman, D. C.; Hutchison, C. A., Jr.; Kohler, B. E.; Stout, J. W. *J. Chem. Phys.* **1965**, *42* (3), 1048.

Table II. Experimental and Calculated g Values for the $\bar{E}$ and $2\bar{A}$ (^2E_g) Excited States

	exptl[a]		
	from bands A and B	from bands C and D	calcd[b]
$g_\parallel(\bar{E})$	2.19	2.11	2.00
$g_\perp(\bar{E})$	0	0	0.00
$g_\parallel(2\bar{A})$		2.14	2.00
$g_\perp(2\bar{A})$	0	0	0.00

[a] Derived from Zeeman experiments. [b] From ref 16.

intensity between 10 and 200 K of 25% ($MgCl_2$) and 40% ($CdCl_2$). This is most likely due to a corresponding increase of absorption intensity in the excitation region (vibronic intensity mechanism). A radiationless relaxation mechanism becomes effective and competitive above 200 K in the $CdCl_2$ host, causing the sharp drop of luminescence intensity. Excitation transfer to quenching traps is ruled out by the observed lack of concentration dependence, as expected for these diluted crystals. Multiphonon relaxation to the ground state is therefore the most likely quenching mechanism.[18] In the simplest possible model the energy difference between the crossing point of the $^4A_{2g}$ and $^4T_{2g}$ potential curves and the bottom of $^4T_{2g}$ can be considered as an activation barrier for nonradiative $^4T_{2g} \rightarrow {}^4A_{2g}$ relaxation. Indeed, this energy difference is much smaller for $Cd_{1-x}V_xCl_2$ than for $Mg_{1-x}V_xCl_2$, which qualitatively explains the observed behavior. Quantitative agreement is not obtained and should not be expected on the basis of this simple model.

In the concentrated material VCl_2 we observe typical solid-state effects as a result of the excitonic nature of $^4A_{2g} \rightarrow {}^4T_{2g}$. Effects such as transfer of excitation energy within the coupled VCl_2 system become possible.[19] The sharp drop of V^{2+} luminescence intensity between 5 and 30 K concurs with the steep rise of an impurity band centered at approximately 4800 cm^{-1}. This band is already present at 5 K. Most likely this low-energy emission arises from a Ni^{2+} impurity, contained in the VCl_2 crystal in a very small concentration. $^3T_{2g} \rightarrow {}^3A_{2g}$ luminescences of Ni^{2+} in fluoride and oxide lattices have been reported in this spectral range.[3,20] We have also observed a Ni^{2+} emission in $CsMg_{1-x}Ni_xCl_3$ centered at 5250 cm^{-1} (6 K).[21] From the measured temperature dependences (Figure 5) it is obvious that the Ni^{2+} luminescence is fed by excitation transfer from the vanadium system. We can deduce an empirical activation energy of 10 cm^{-1} for the overall $V^{2+} \rightarrow Ni^{2+}$ transfer process from the Arrhenius plot of the low-temperature data in Figure 5 (insert). It is more likely that this activation barrier corresponds to the $V^{2+} \rightarrow V^{2+}$ than to the $V^{2+} \rightarrow Ni^{2+}$ transfer step. The $^3A_{2g} \rightarrow {}^3T_{2g}$ absorption of a $NiCl_6^{4-}$ center peaks at approximately 7000 cm^{-1}. It is thus practically coincident with the VCl_6^{4-} emission (Figure 4). The spectral overlap, which determines the nonradiative $V^{2+} \rightarrow Ni^{2+}$ transfer efficiency, is therefore a maximum. For the $V^{2+} \rightarrow V^{2+}$ step, on the other hand, relaxation of the excited V^{2+} center into the $^4T_{2g}$ potential minimum will lead to a thermally activated transfer because of the different equilibrium geometries.

4.2. Luminescence Fine Structure. A progression in the totally symmetric VCl_6 breathing mode is a common feature of all three luminescence spectra below 10 K. The region of electronic $^4T_{2g} \rightarrow {}^4A_{2g}$ origins is resolved only in the dilute systems. The true origins and their associated a_{1g} progression have magnetic dipole character. They are relatively more intense in the $MgCl_2$ host.

Besides the dominant a_{1g} progression we observe a progression also in the e_g mode. It clearly indicates a dynamical Jahn–Teller effect in the excited $^4T_{2g}$ state. From the observed intensity distributions within the a_{1g} and e_g modes in the luminescence spectrum we can obtain an estimate of the geometrical distortions in the emitting state. Values of the Huang–Rhys factor, defined

(18) Dexter, D. L.; Klick, C. C.; Russel, G. A. *Phys. Rev.* **1955**, *100* (2), 603.
(19) Powell, R. C.; Blasse, R. *Struct. Bonding (Berlin)* **1980**, *42*, 43.
(20) Iverson, M. V.; Sibley, W. A. *J. Lumin.* **1979**, *20*, 311.
(21) Reber, C., unpublished work.

Table III. Parameters Characterizing the Shapes and Relative Positions of $^4A_{2g}$ and $^4T_{2g}$ Potential Curves along the a_{1g} and e_g Coordinates[a]

host lattice	E_{max}, cm^{-1} absorption	E_{max}, cm^{-1} emission	Stokes shift, cm^{-1}	$^4A_{2g}$ state a_{1g} freq, cm^{-1}	$^4A_{2g}$ state e_g freq, cm^{-1}
$MgCl_2$	9330	7420	1910	240	209
$CdCl_2$	9000	6850	2250	220	185

$S_{a_{1g}}$	S_{e_g}	$\Delta A_{a_{1g}}$, Å	ΔQ_{e_g}, Å	host lattice
4	1.0	0.25	−0.11	$MgCl_2$
4.5	1.7	0.28	−0.16	$CdCl_2$

[a] All the values given correspond to temperatures of 10 K or below. S_i (Huang–Rhys factor) and ΔQ_i values were estimated from the intensity distribution within the progressions in Figure 6.

as $S = n \cdot I_n/I_{n-1}$ (n numbers the members of the progression), are included in Table III. Excited-state distortions ΔQ_i along the coordinates i = a_{1g}, e_g are calculated by using the relations in ref 22 and 23. ΔQ_i values are collected in Table III. The $\Delta Q_{a_{1g}}$ values are larger than ΔQ_{e_g} for both host lattices. The excited state is spatially more extended in the $CdCl_2$ host lattice, in nice correspondence with the greater size of the Cd^{2+} ion. Jahn–Teller energies E_{JT} of 209 and 310 cm^{-1} are calculated for $Mg_{1-x}V_xCl_2$ and $Cd_{1-x}V_xCl_2$, respectively. There are only rough estimates due to rather large errors in the intensity values. In $Mg_{1-x}V_xCl_2$ we have another handle on the Jahn–Teller effect, which will be used for comparison in the next paragraph.

The $^4T_{2g}$ state is energetically split by a trigonal crystal field component and spin–orbit coupling. The trigonal splitting equals $3K/2$. From the EPR results[17] we derive a spin–orbit parameter value $\zeta = 100$ cm^{-1}. An estimate for K of −270 cm^{-1} is obtained from the energy difference of the $^4A_{2g} \rightarrow {}^4T_{1g}{}^a$ absorption maxima in σ and π polarization. These parameters (Table I) also reproduce the observed splitting of the ^2E_g level. The $^4T_{2g}$ splitting can be represented by the effective Hamiltonian[24]

$$H_{eff} = \lambda(\vec{L}\vec{S}) + \kappa(\vec{L}\vec{S})^2 + \sigma(L_x^2S_x^2 + L_y^2S_y^2 + L_z^2S_z^2) + V_{trig} \quad (1)$$

Reasonable spin–orbit parameter values λ, κ, σ can be estimated by fitting the eigenvalues of eq 1 to the $^4T_{2g}$ spin–orbit splitting obtained from a full octahedral d^3 crystal field calculation and the parameters in Table I. With the parameter values $\lambda = -15.6$ cm^{-1}, $\kappa = 1.2$ cm^{-1}, $\sigma = 4.0$ cm^{-1}, and $K = -270$ cm^{-1}, appropriate for $Mg_{1-x}V_xCl_2$, the lower lying trigonal component $^4E_g(T_{2g})$ is calculated to split into four spin–orbit components with energy differences of 13.6, 29.2, and 46.3 cm^{-1}. Experimentally we find a total spread of the four lowest-energy $^4T_{2g} \rightarrow {}^4A_{2g}$ transitions of 19 cm^{-1} in $Mg_{1-x}V_xCl_2$. This is much smaller than theoretical expectations, independent of the somewhat ambiguous choice of K. We interpret this quenching of the spin–orbit splitting as a Ham effect resulting from the Jahn–Teller vibronic coupling.[24] In a procedure analogous to that used for the octahedral $CrCl_6^{3-}$ complex[22] we can calculate the Ham quenching. The Ham quenching factor λ is related to the Jahn–Teller energy E_{JT} by the expression

$$\gamma = e^{-3E_{JT}/2\hbar\omega}$$

where $\hbar\omega$ is the e_g energy.

A reasonable reproduction of the observed energy splitting is obtained for $\gamma = 0.39$, corresponding to a Jahn–Teller energy of 130 cm^{-1}. This is more reliable than the Jahn–Teller energy of 209 cm^{-1} estimated from the intensity distribution in the e_g progression. The Jahn–Teller energies are of the same order of magnitude as K for both host lattices. In our theoretical model the trigonal crystal field has been considered to first order only, which is obviously a poor theoretical approximation to our physical situation. But even without going any further, we conclude that there is multiple experimental evidence for a Jahn–Teller effect in the $^4T_{2g}$ state of V^{2+} in $MgCl_2$ and $CdCl_2$. The Jahn–Teller distortion is smaller in the $MgCl_2$ host, most likely as a result of the smaller size of the Mg^{2+} ion.

4.3. ^2E_g and $^2T_{1g}$ Excitations. The spectral region between 11 500 and 13 000 cm^{-1} in absorption corresponds to the spin-forbidden ^2E_g and $^2T_{1g}$ transitions. They are 1–2 orders of magnitude more intense in VCl_2 than in the diluted materials. This intensity enhancement in the antiferromagnetic material is undoubtedly due to an exchange mechanism,[25] and the bands are assigned as magnon sidebands and magnon–phonon sidebands. The origins are not observed in the VCl_2 spectrum. The two relatively sharp bands at 11 470 and 12 150 cm^{-1} have a temperature dependence (Figure 9) that follows the degree of long-range magnetic order. The Neel point of VCl_2 was determined as $T_N = 36$ K,[10] and in Figure 9 the intensity of the two bands is seen to drop toward zero at this temperature. In contrast, the broad sidebands to higher energy retain intensity above 40 K. We therefore assign the bands at 11 470 and 12 150 cm^{-1} to magnon sidebands of ^2E_g and $^2T_{1g}$, respectively, with the corresponding magnon reflecting the long-range magnetic order. The broader bands to higher energy, on the other hand, reflect short-range spin correlations, which extend to much higher temperature than T_N.

The single-ion V^{2+} spectrum is represented by the diluted systems. The bands are extremely sharp and weak, and as shown in section 3 and Figure 10, a full analysis of the ^2E_g transitions can be made on the basis of a simple crystal field model. No analysis was attempted for the rather complicated $^2T_{1g}$ line pattern.

Acknowledgment. This work was financially supported by Swiss National Science Foundation.

(22) Snellgrove, T.; Güdel, H. U. *Inorg. Chem.* **1978**, *17*, 1617.
(23) Wilson, R. B.; Solomon, E. I. *J. Am. Chem. Soc.* **1980**, *102*, 4087.
(24) Sturge, M. D. *Solid State Phys.* **1967**, *20*, 91.
(25) Tanabe, Y.; Moriya, T.; Sugano, S. *Phys. Rev. Lett.* **1965**, *15* (26), 1023.